remote sensing

MDPI

Article

Winter Precipitation Detection Using C- and X-Band Radar Measurements

Ayano Ueki [1,2,*], Michihiro S. Teshiba [1,†], David Schvartzman [2,3,4], Pierre-Emmanuel Kirstetter [2,3], Robert D. Palmer [2,3,4], Kohei Osa [1], Tian-You Yu [2,3,4], Boonleng Cheong [2,4] and David J. Bodine [2,3]

[1] Weathernews Inc., Chiba 261-0023, Japan; msteshiba@gmail.com (M.S.T.); osa@wni.com (K.O.)
[2] Advanced Radar Research Center, University of Oklahoma, Norman, OK 73019, USA; dschvart@ou.edu (D.S.); pierre-emmanuel.kirstetter@ou.edu (P.-E.K.); rpalmer@ou.edu (R.D.P.); tyu@ou.edu (T.-Y.Y.); boonleng@ou.edu (B.C.); bodine@ou.edu (D.J.B.)
[3] School of Meteorology, University of Oklahoma, Norman, OK 73019, USA
[4] School of Electrical and Computer Engineering, University of Oklahoma, Norman, OK 73019, USA
* Correspondence: aueki@ou.edu
† Current address: EKO instruments Co., Ltd., Tokyo 151-0072, Japan.

Abstract: Winter continues to witness numerous automobile accidents attributed to graupel and hail precipitation in Japan. Detecting these weather phenomena using radar technology holds promise for reducing the impact of such accidents and improving road maintenance operations. Weather radars operating at different frequencies, such as C- and X-band, prove effective in graupel detection by analyzing variations in backscattered signals within the same radar volume. When particle diameters exceed 5 mm, the study of Mie scattering characteristics across different melting ratios reveals insights. The dual frequency ratio (DFR) shows potential for graupel detection. The DFR presents wider variations with ten-times difference in melting ratios with increased density, offering opportunities for precise detection. Additionally, the DFR amplitude rises with temperature changes. However, for hydrometeor diameters below approximately 3 mm, and within the Rayleigh region, the DFR exhibits minimal fluctuations. Hence, this technique is best suited for diameters exceeding 3 mm for optimal efficacy. Additionally, a "detection alert" for graupel/hail has been proposed. Based on this alert, and with realistic rain/graupel size distributions, graupel/hail can be detected with an approximate probability of 70%.

Keywords: graupel detection; dual frequency ratio; multiple frequency weather radar

check for updates

Citation: Ueki, A.; Teshiba, M.S.; Schvartzman, D.; Kirstetter, P.-E.; Palmer, R.D.; Osa, K.; Yu, T.-Y.; Cheong, B.; Bodine, D.J. Winter Precipitation Detection Using C- and X-Band Radar Measurements. *Remote Sens.* **2024**, *16*, 2630. https://doi.org/10.3390/rs16142630

Academic Editor: Gad Levy

Received: 20 June 2024
Revised: 12 July 2024
Accepted: 16 July 2024
Published: 18 July 2024

Copyright: © 2024 by the authors. Licensee MDPI, Basel, Switzerland. This article is an open access article distributed under the terms and conditions of the Creative Commons Attribution (CC BY) license (https://creativecommons.org/licenses/by/4.0/).

1. Introduction

Classification of hydrometeor types on the ground are paramount for ensuring safe and efficient ground transportation, particularly in Japan where graupel and/or hail-fall events can lead to significant disruptions, including road closures and train stoppages. As depicted in Figure 1, between 2008 and 2011, over 100 severe car accidents were attributed to graupel-fall events [1]. The temporal and spatial extent of graupel-fall is highly limited and localized, posing challenges for detection compared to typical rainfall/snowfall events.

Given that the detection of graupel and/or hail-fall is performed aloft, the alert of the detection is shed beforehand, because the lead time of the alert is extremely important for the anticipation of disasters. However, the quantification of hydrometeor types is most challenging using radar observations, because real-time comparisons between radar and in situ observations aloft are also difficult to conduct. In pursuit of detecting and classifying hydrometeors aloft, dual-polarization weather radars have been instrumental (e.g., [2]). These radars can measure differences between radar reflectivity in horizontal (H) and vertical (V) polarizations, quantified by differential reflectivity Z_{DR}, and phase differences denoted by differential phase Φ_{DP}. Combining these dual-polarization variables yields insights into hydrometeor types through theoretical models (e.g., [3,4]) or techniques

such as fuzzy-logic-based classifications (e.g., [5,6]). To facilitate real-time analysis of weather conditions, the Japanese government is currently deploying C- and X-band dual-polarization weather radars nationwide [7].

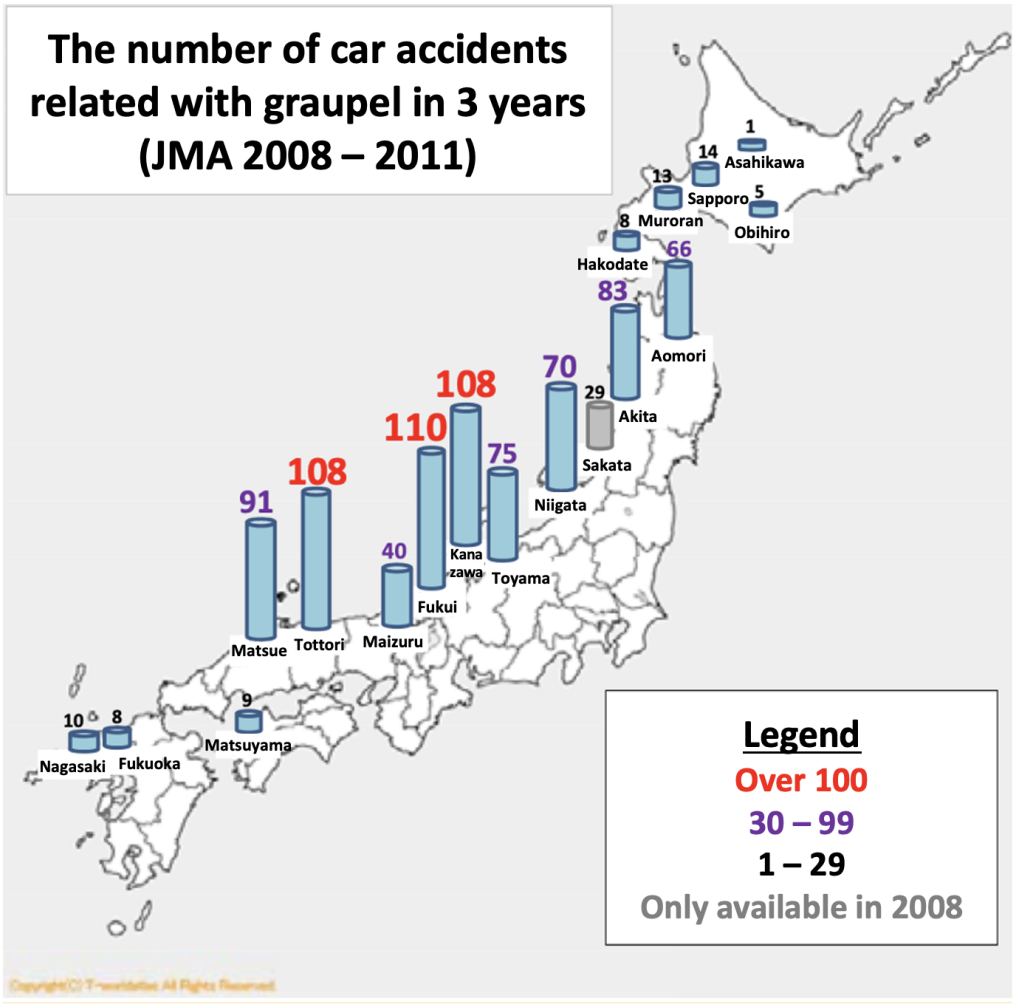

Figure 1. Occurrences of car accidents caused by graupel-/hail-fall events (translated from [1] into English).

Another strategy for detecting graupel and hail leverages differences in scattering characteristics observed by multi-frequency weather radars. These radars combine various bands such as S- and C-bands (e.g., [8–11], S- and X-bands (e.g., [12]), and C- and X-bands. Utilizing multi-frequency detection algorithms precludes the need for dual polarization measurements, simplifying radar design and allowing compatibility with existing networks that may lack polarimetric capabilities. In Japan, Weathernews Inc. (headquarter is located in Chiba, Japan) (WNI), a private weather forecasting company, is deploying low-cost single-polarization X-band weather radars with considerable flexibility and control [13], which may enhance graupel detection capabilities.

The Japanese government has deployed C-band weather radars for operational weather surveillance. These have pre-defined scan strategies and waveforms due to operational imperatives. This study aims to enhance graupel detection capabilities by amalgamating data from Japan's operational C-band radars with data from private-sector X-band radars.

Scattering at C- and X-bands often exceeds the Rayleigh region, particularly for hydrometeors the size of graupel and hail. Consequently, these wavelengths are conducive to detection and classification algorithms.

Figure 2 illustrates the radar cross-section as a function of diameter of liquid spherical particles for C- and X-band radars. The radar cross-sections of the horizontal plane are calculated using the T-matrix method [14]. Notably, the radar cross-section ratio between the C- and X-bands deviates from a constant for diameters exceeding approximately 10 mm, as depicted in regions beyond Rayleigh scattering (diameters below 5 mm). This discrepancy in backscattering cross-sections between C- and X-bands offers a basis for identifying graupel.

The dual-frequency ratio (DFR), akin to the dual-wavelength ratio, characterizes differences in backscattering across different operational frequencies or wavelengths. DFR is influenced by differential backscattering and varies based on particle types such as rain, snow, and graupel, and size, orientation, rime fraction, and radar beam characteristics. The DFR has found applications in multi-frequency radar measurements for microphysical retrievals, including estimations of liquid water content (e.g., [15,16]), snowfall rate (e.g., [17]), graupel and hail detection (e.g., [18]), and hydrometeor classification (e.g., [19–23].

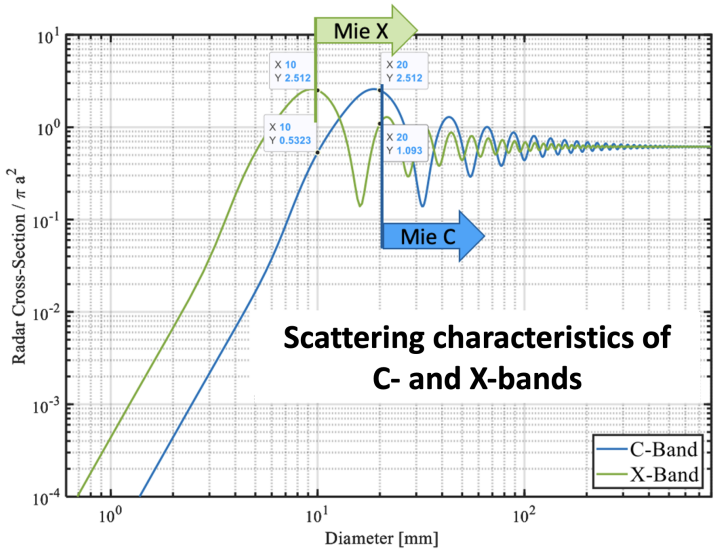

Figure 2. Radar cross-section in diameter of particles with C- and X-band frequencies.

It should be emphasized that the detection alert for graupel/hail does not involve the phase of hydrometeors, except for the pure water phase. The condition for the alert is that rain contamination is not present, although some graupel/hail cases may not be detected.

In this article, we apply hydrometeors backscattering theory as a function of mixture of water and solid ice changes and how scattering would follow the changes. In the next section, the definition of the DFR with associated theory behind radar cross-section and dielectric constants will be given. Preliminary simulation results related to the detection alert are provided in Section 3, along with conclusions and future plans in Section 4.

2. Methodology

2.1. Dual-Frequency Ratio

The radar equation as related to the radar reflectivity Z is shown as:

$$Z = \frac{\lambda^4}{\pi^5 |K|^2} \int_0^\infty N(D)\, \sigma_b(D) dD \tag{1}$$

where $N(D)$ is the particle size distribution in the equivolume diameters between D and $D + dD$, and λ is the wavelength [24,25]. The terms of this equation correspond to the characteristics of hydrometeors are the total sum of backscattering cross-section of hydrometeors σ_b and the complex value of the dielectric factor $|K|^2$. Additionally, given that this equation is applied to the each operational frequency such as the C- and X-band, the wavelengths λ are also different. Other terms are particular for each radar, and these

should be calibrated when the reflectivity factor Z is used for calculation of the dual frequency ratio. The DFR is defined hereafter by a ratio between the linear reflectivity factors with the same polarization of X- and C-band radars. Typically, as the weather observation is conducted with the horizontal polarization, the reflectivity factors have the horizontal polarization.

The fundamental benefit of the DFR is that it shows the potential of the estimation of hydrometeors types and sizes in the common volume of the beams of each radar. Assuming the radar volumes are almost the same size and location for each radar, the distribution of hydrometeors in the volumes is uniform, therefore the backscattering cross-section of hydrometeors can be assumed to have similar characteristics. Hence, the difference between the reflectivity factors of different frequencies comes from the scattering mechanisms of hydrometeors. Note that the radar reflectivity observed in each radar should be well-calibrated. Therefore, frequency differences between radars may result in resolution volumes with different sizes, which affects the computed DFRs. Furthermore, there are some limitations of the radar scan configurations for operational government-owned weather radars, and the dual-polarization variables observed by the Japanese government-owned C-band radars have not been open for realtime access.

2.2. Potential Application of DFR

The scattering cross-section of hydrometeors undergoes changes influenced by factors such as hydrometeor diameter and shape, and the total sum of the scattering cross-sections is affected by the number density and ice density. The mixture ratio of water and ice particles varies according to ambient temperature, impacting the complex dielectric constants associated with water and ice types. In this study, parameters including hydrometeor diameter, ice density, and the water–ice mixture ratio are analyzed to assess changes in backscattering cross-sections and the complex dielectric constants of water and ice.

Furthermore, the investigation extends to the examination of different hydrometeor types, given the distinct backscattering mechanisms inherent in Rayleigh and Mie scatterings, which can influence the DFR. Lastly, considering the significance of graupel in road maintenance operations and forecasting, this study delves into the characteristics of graupel.

2.3. Characteristics of Graupel

Several observational research projects have been conducted to investigate the characteristics of graupel. As a reference, the diameter of graupel is approximately between 2 and 5 mm, defined by [26], and given the diameter range is provided, the density of graupel is also defined as 0.3 g/cm^3, which is adopted by the mean observational values reported ([27,28]). These conditions are adopted here for the calculations of dielectric constants.

2.4. Backscattering Cross-Section and DFR

In order to simplify the hypothesis, the backscattering cross-section is calculated for one particle and spherical shape, and inclusion of water and ice will be described as the volume ratio in one particle, because the size of radar volume is much larger than that of cross-section. As the densities and melting characteristics in water and ice are different, air, water, and ice can be specifically characterized by the complex dielectric constant or permittivity $\epsilon = \mathrm{Re}(\epsilon) + j\mathrm{Im}(\epsilon)$. The complex dielectric factor is calculated using the the formula:

$$K = \frac{\epsilon_e - 1}{\epsilon_e + 2} \tag{2}$$

where ϵ_e is the effective dielectric constant. The relative dielectric constant of air ϵ_a, ice ϵ_i, and water ϵ_w are calculated from the Debye theory [29] with the functions of temperature, phase of water, and operational frequencies of 5.6 GHz (C-band) and 10 GHz (X-band).

On the other hand, the densities of wet snow ρ_{ws}, dry snow ρ_{ds}, and water ρ_w have the relationship of the melting ratio of particles γ:

$$\rho_{ws} = \rho_{ds}(1-\gamma^2) + \rho_w\gamma^2. \tag{3}$$

Melting ratios vary between 0 and 1, which means that the particles are either frozen or melted. As the density of wet snow can be given, the fractional volumes are calculated as:

$$f_w = \gamma\frac{\rho_{ws}}{\rho_w} \tag{4}$$

$$f_i = (1-\gamma)\frac{\rho_{ws}}{\rho_i} \tag{5}$$

$$f_a = 1 - f_i - f_w. \tag{6}$$

The dielectric constant of air depends on atmospheric pressure, temperature, and humidity, and so it is slightly different from unity. A dielectric constant is the measure of the influence of a polarized electric field, polarizability, in response to an electric field [30], therefore a effective dielectric constant ϵ_e is shown as below:

$$\frac{\epsilon_e}{\epsilon_1} = \frac{1 + 2N\alpha/3\epsilon_1\epsilon_0}{1 - N\alpha/3\epsilon_1\epsilon_0} \tag{7}$$

where N is the number of dipoles per unit volume, α is the polarizability of the sphere, ϵ_1 is the relative dielectric constant for the background medium, ϵ_0 is the dielectric constant in a free space, and V is the volume of the sphere. A fractional volume $f = NV$ introduces to the equation of an effective dielectric constant, and the polarizability of the sphere

$$\alpha = \frac{\epsilon_2 - \epsilon_1}{\epsilon_2 + 2\epsilon_1} 3\epsilon_1\epsilon_0 V, \tag{8}$$

then the effective dielectric constant is rewritten as:

$$\frac{\epsilon_e}{\epsilon_1} = \frac{1 + 2fy}{1 - fy} \tag{9}$$

with

$$y = \frac{\epsilon_2 - \epsilon_1}{\epsilon_2 + 2\epsilon_1}. \tag{10}$$

This equation is referred to as Maxwell-Garnett (M-G) mixing formula under the condition of $fy \ll 1$. In the case of graupel [30], the media of air, ice, and water have the relative dielectric constants of ϵ_a, ϵ_i, and ϵ_w, and their fractional volumes are f_a, f_i and f_w, respectively. The fractional volumes have the relationship of $f_a + f_i + f_w = 1$. The calculation of the relative dielectric constants follows the procedure shown below [30]:

1. Let $\epsilon_1 = \epsilon_a$ and $\epsilon_2 = \epsilon_i$. Then, calculate their fractional volumes in the two-medium mixture with $f_1 = \dfrac{f_a}{(f_a + f_i)}$ and $f_2 = 1 - f_1$.
2. Calculate the effective dielectric constant $\epsilon_{ai} = \epsilon_e$ for the air–ice mixture (dry snow or graupel) using the M-G formula with $f = f_2$.
3. Let $\epsilon_1 = \epsilon_w$ and $\epsilon_2 = \epsilon_{ai}$. Then, determine their fractional volumes of water and dry snow or graupel with $f_1 = f_w$ and $f_2 = 1 - f_w$.
4. Repeat 2 to obtain the effective dielectric constants for the three-medium mixture.

After this process, the effective dielectric constant of three medium mixture ϵ_{aiw} is calculated, then can be applied to the complex dielectric factor K.

3. Simulation Results

As indicated previously, the DFR is a function of melting ratio, density, and temperature. In this study, the temperature range is varied between −6 °C and 3 °C, corresponding to graupel conditions. This range aligns with the seasonal-minimum monthly mean temperature recorded at Wajima observatory in Japan during the period of 1991–2020, which was −4.2 °C at a geopotential height of 1 km and 3 °C at ground level [31]. Assuming a density equal to unity implies that all particles are melted, thus resulting in a melting ratio of unity. However, the DFR calculations can yield melting ratios other than unity.

Initial results of the DFR simulations are depicted in Figures 3 and 4. For particles with diameters exceeding 5 mm, the characteristics of Mie scattering become apparent in specific melting ratios. Higher densities lead to elevated DFR values across a broader melting ratio range, offering opportunities to discern variations in melting ratio through the DFR. Moreover, the amplitude of the DFR increases with temperature changes. In diameters below 3 mm, within the Rayleigh region, the DFR exhibits minimal variation. Hence, for optimal efficacy, this technique should be applied to diameters exceeding 3 mm.

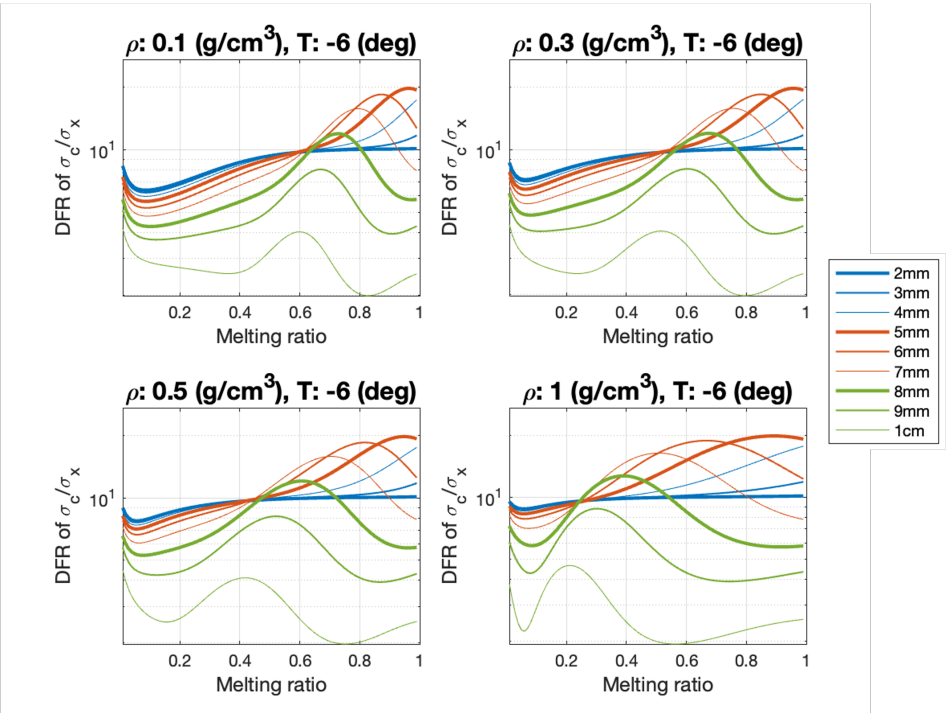

Figure 3. DFR changes in melting ratio with respect to densities of 0.1, 0.3, 0.5, and 1 g/cm^3 in the temperature of −6 °C. The X-axis represents the melting ratio of hydrometeors, and the Y-axis represents the DFR of the radar backscattering cross-sections at C-band (σ_C) and X-band (σ_X) radar frequencies.

In order to use the DFR for detecting graupel and hail, we need to define the alert threshold. Given that the graupel density is approximately 0.3 g/cm^3, we can calculate the probability of graupel detection as follows.

The DFR exhibits an offset corresponding to the DSDs of graupel and rain. The DSDs of graupel and rain $N(D)$ [m^{-4}] are described by the following equations:

$$N(D) = N_0 \exp(-\lambda D) \tag{11}$$

where N_0 [m^{-4}] is the intercept parameter, with values 4×10^6 [m^{-4}] for graupel and 8×10^6 [m^{-4}] for rain. Here, D is the diameter of the particles, and λ is the slope parameter, which follows the graupel/rain mixing ratio with air and is given by the following equation [32]:

$$\lambda = \left(\frac{\pi \rho_p N_0}{\rho q_p} \right)^{0.25} \tag{12}$$

where ρ_p is the density of graupel/rain particles, ρ is the air density, and q_p is the mixing ratio of graupel/rain with air. The melting ratio γ is calculated by the ratio of the mixing ratio of rain to the total mixing ratio of graupel and rain, $\gamma = q_r/(q_r + q_g)$. Figure 4 illustrates this process.

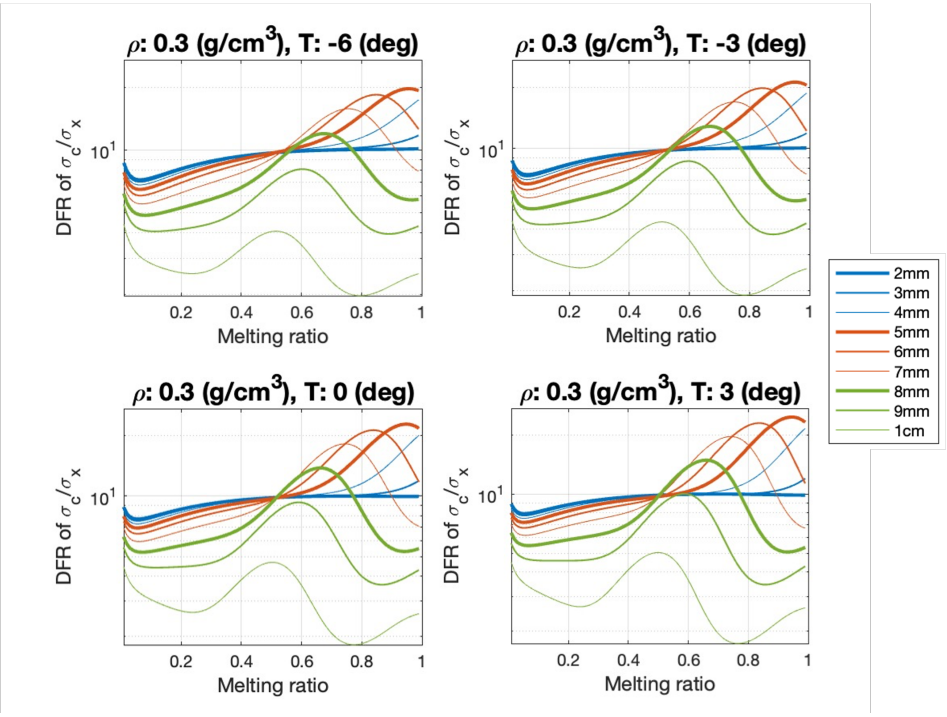

Figure 4. DFR changes in melting ratio with respect to temperatures of −6, −3, 0, and 3 °C in the density of 0.3 g/cm^3. The X-axis represents the melting ratio of hydrometeors, and the Y-axis represents the DFR of the radar backscattering cross-sections at the radar frequencies of C-band (σ_C) and X-band (σ_X).

We define three thresholds based on the mixing status of rain (water) and graupel/hail (ice): the minimum threshold, the rain threshold, and the maximum threshold. The graupel/hail detection alert is triggered when the observed DFR exceeds the specified threshold. If the alert is applied below the minimum threshold, it can detect all graupel/hails in any mixed phase, but may also include rain contamination, as the DFR exceeds the alert threshold when the mixing ratio equals one. When the alert is between the minimum and the rain threshold, false alerts may occur in rain cases, and some graupel/hail detections may be missed because the DFR for some graupel/hail cases is below the alert threshold. We calculate the percentage of missed graupel/hail relative to the total, referred to as the "Missing Ratio". Setting the graupel/hail alert above the rain threshold ensures no contamination from rain and avoids false alerts related to rain, although the missing ratio may increase. Once the alert exceeds the maximum threshold, it becomes impossible to detect graupel/hail. Figure 5 summarizes potential graupel/hail alert candidates in Table 1. Graupel/hail alerts can be triggered at various temperatures and in different mixed phases. When set at the rain threshold, the missing ratio ranges between 21% and 38%, with detection percentages ranging from 62% to 79%. The graupel/hail alert can be applied in ambient temperatures and must account for potential missed alerts for graupel/hail and false alerts for rain.

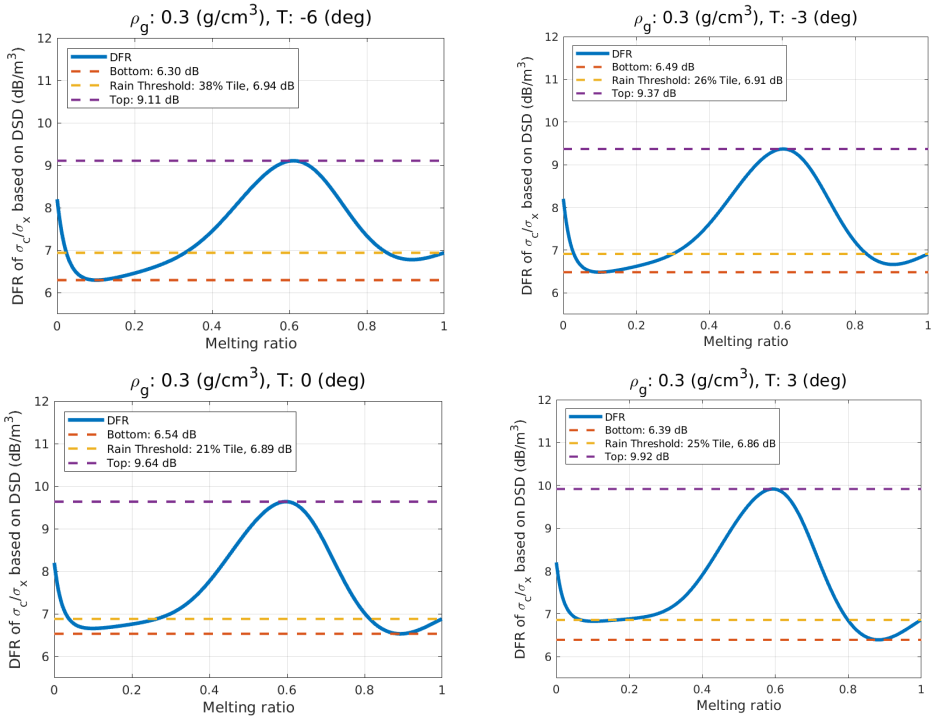

Figure 5. Possibilities of graupel detection with DFR with respect to temperatures of −6, −3, 0, and 3 °C in the density of 0.3 g/cm^3.

Table 1. Summary of the thresholds for the detection alert.

Temperature (°C)	Minimum Threshold (dB/m^3)	Rain Threshold		Maximum Threshold (dB/m^3)
		DFR (dB/m^3)	Missing Ratio %	
−6	6.30	6.94	38	9.11
−3	6.49	6.91	26	9.37
0	6.54	6.89	21	9.64
3	6.39	6.86	25	9.92

4. Summary and Future Work

During Japan's winter season, automobile accidents are frequent due to the hazardous conditions caused by graupel and hail. Detecting the formation of graupel and hail aloft is imperative for alerting drivers and minimizing accidents. Leveraging multiple weather radars equipped with diverse operational frequencies proves effective in discerning variations in backscattering mechanisms within the same radar volume across multiple frequencies.

When particles exceed a diameter of approximately 5 mm, they exhibit distinctive characteristics of Mie scattering, particularly evident in the specific melting ratio. Higher densities result in elevated DFR within a broader melting ratio range, offering an opportunity to discern variations in melting ratio alongside the DFR. As temperature fluctuates, the amplitude of the DFR correlates positively, amplified with rising temperatures. Conversely, in diameters below approximately 3 mm, within the Rayleigh region, the DFR experiences minimal variation. Hence, this technique is best suited for diameters exceeding 3 mm to yield optimal results.

The preliminary results presented offer promising avenues for estimating the likelihood of graupel or hail fall in Japan, as discernible DFR signatures across various radar frequencies have emerged under specific conditions. There is the possibility to make a graupel/hail alert for several temperatures and various mixed phases. Given that the graupel/hail alert is set at the rain threshold, the detection percentage is approximately 70%.

This paper provides the criteria of a new graupel/hail alert with respect to the DFR. Future investigations will explore the potential of detection based on hypotheses surrounding graupel size distribution. Subsequently, the efficacy of the DFR technique will be assessed using real observational datasets obtained from C- and X-band weather radars. For the application of this method on real datasets, several factors must be considered. Differences in radar reflectivity between two radar frequencies may occur due to attenuation caused by large hydrometeor diameters. It is essential that both radars are well calibrated and that the radar volumes are matched. Additionally, because there is a gap between the radar volume and the ground, the phase of the hydrometeors aloft may differ from that observed on the ground. Some of these errors, such as the uncertainty in cross-calibration and random measurement errors, can be theoretically modeled, but it may be difficult to model others. Future research and development are necessary. Lastly, the eventual combination of this DFR-based detection method with dual-polarization measurements could yield superior graupel detection capability.

Author Contributions: Conceptualization, A.U., D.S., M.S.T., R.D.P., K.O., T.-Y.Y., B.C., P.-E.K. and D.J.B.; methodology, A.U., D.S., K.O. and M.S.T.; software, A.U. and D.S.; validation, D.S., K.O. and M.S.T.; formal analysis, A.U., D.S., K.O. and M.S.T.; investigation, A.U. and D.S.; resources, A.U., D.S. and M.S.T.; writing—original draft preparation, A.U., M.S.T., D.S. and R.D.P.; writing—review and editing, K.O., T.-Y.Y., B.C., P.-E.K. and D.J.B.; visualization, A.U., D.S. and M.S.T.; supervision, D.S.; project administration, D.S.; funding acquisition, D.S. and R.D.P. All authors have read and agreed to the published version of the manuscript.

Funding: This work was funded by Weathernews Inc. through a collaboration with East Nippon Expressway Co., Ltd. (headquarter is located in Tokyo, Japan) (NEXCO EAST).

Institutional Review Board Statement: Not applicable.

Informed Consent Statement: Not applicable.

Data Availability Statement: Data are contained within the article.

Conflicts of Interest: The authors declare no conflicts of interest. The funders had no role in the design of the study; in the collection, analyses, or interpretation of data; in the writing of the manuscript; or in the decision to publish the results.

References

1. Yatsuo, T.; Hattori, H.; Okura, T.; Aiba, Y. Operation and effectiveness of an information-providing system using graupel detection. In Proceedings of the Yukimirai Conference, Akita, Japan, 7–8 February 2013. (In Japanese)
2. Zrnic, D.S.; Ryzhkov, A.V. Polarimetry for Weather Surveillance Radars. *Bull. Am. Meteorol. Soc.* **1999**, *80*, 389–406. [CrossRef]
3. Straka, J.M.; Zrnić, D.S.; Ryzhkov, A.V. Bulk Hydrometeor Classification and Quantification Using Polarimetric Radar Data: Synthesis of Relations. *J. Appl. Meteorol.* **2000**, *39*, 1341–1372. [CrossRef]
4. Dolan, B.; Rutledge, S.A. A Theory-Based Hydrometeor Identification Algorithm for X-Band Polarimetric Radars. *J. Atmos. Ocean. Technol.* **2009**, *26*, 2071–2088. [CrossRef]
5. Park, H.S.; Ryzhkov, A.V.; Zrnić, D.S.; Kim, K.E. The Hydrometeor Classification Algorithm for the Polarimetric WSR-88D: Description and Application to an MCS. *Weather Forecast.* **2009**, *24*, 730–748. [CrossRef]
6. Thompson, E.J.; Rutledge, S.A.; Dolan, B.; Chandrasekar, V.; Cheong, B.L. A Dual-Polarization Radar Hydrometeor Classification Algorithm for Winter Precipitation. *J. Atmos. Ocean. Technol.* **2014**, *31*, 1457–1481. [CrossRef]
7. Japan Meteorological Agency Home Page. Weather Radar Observation. Available online: https://www.jma.go.jp/jma/en/Activities/radar/radar.html (accessed on 6 November 2023).
8. Féral, L.; Sauvageot, H.; Soula, S. Hail Detection Using S- and C-Band Radar Reflectivity Difference. *J. Atmos. Ocean. Technol.* **2003**, *20*, 233–248. [CrossRef]
9. Kaltenboeck, R.; Ryzhkov, A.V. Comparison of polarimetric signatures of hail at S and C bands for different hail sizes. In Proceedings of the 6th European Conference on Severe Storms 2011, Palma de Mallorca, Spain, 3–7 October 2011.
10. Picca, J.; Ryzhkov, A. A Dual-Wavelength Polarimetric Analysis of the 16 May 2010 Oklahoma City Extreme Hailstorm. *Mon. Weather Rev.* **2012**, *140*, 1385–1403. [CrossRef]
11. Junyent, F.; Chandrasekar, V.; Bringi, V.N.; Rutledge, S.A.; Kennedy, P.C.; Brunkow, D.; George, J.; Bowie, R. Transformation of the CSU–CHILL Radar Facility to a Dual-Frequency, Dual-Polarization Doppler System. *Bull. Am. Meteorol. Soc.* **2015**, *96*, 975 – 996. [CrossRef]

12. Witt, A.; Burgess, D.W.; Seimon, A.; Allen, J.T.; Snyder, J.C.; Bluestein, H.B. Rapid-Scan Radar Observations of an Oklahoma Tornadic Hailstorm Producing Giant Hail. *Weather Forecast.* **2018**, *33*, 1263–1282. [CrossRef]
13. Teshiba, M.S.; Abe, D. X-band Operational Weather Radar Network for Early Warnings of Rainfall/Snowfall Disasters. In Proceedings of the 40th AMS Conference on Radar Meteorology, Minneapolis, MN, USA, 28 August–1 September 2023.
14. Waterman, P. Matrix formulation of electromagnetic scattering. *Proc. IEEE* **1965**, *53*, 805–812. . [CrossRef]
15. Huang, D.; Johnson, K.; Liu, Y.; Wiscombe, W. High resolution retrieval of liquid water vertical distributions using collocated Ka-band and W-band cloud radars. *Geophys. Res. Lett.* **2009**, *36*. [CrossRef]
16. Zhu, Z.; Lamer, K.; Kollias, P.; Clothiaux, E.E. The Vertical Structure of Liquid Water Content in Shallow Clouds as Retrieved From Dual-Wavelength Radar Observations. *J. Geophys. Res. Atmos.* **2019**, *124*, 14184–14197. [CrossRef]
17. Matrosov, S.Y. A Dual-Wavelength Radar Method to Measure Snowfall Rate. *J. Appl. Meteorol.* **1998**, *37*, 1510–1521. [CrossRef]
18. Junyent, F.; Chandrasekar, V.; Kennedy, P. Resonance Scattering Detection Using the CSU–CHILL Dual-Wavelength, Dual-Polarization Radar. *J. Atmos. Ocean. Technol.* **2019**, *36*, 1177–1198. [CrossRef]
19. Kneifel, S.; von Lerber, A.; Tiira, J.; Moisseev, D.; Kollias, P.; Leinonen, J. Observed relations between snowfall microphysics and triple-frequency radar measurements. *J. Geophys. Res. Atmos.* **2015**, *120*, 6034–6055. [CrossRef]
20. Leinonen, J.; Moisseev, D. What do triple-frequency radar signatures reveal about aggregate snowflakes? *J. Geophys. Res. Atmos.* **2015**, *120*, 229–239. [CrossRef]
21. Moisseev, D.N.; Lautaportti, S.; Tyynela, J.; Lim, S. Dual-polarization radar signatures in snowstorms: Role of snowflake aggregation. *J. Geophys. Res. Atmos.* **2015**, *120*, 12644–12655. [CrossRef]
22. Matrosov, S.Y.; Maahn, M.; de Boer, G. Observational and Modeling Study of Ice Hydrometeor Radar Dual-Wavelength Ratios. *J. Appl. Meteorol. Climatol.* **2019**, *58*, 2005–2017. [CrossRef]
23. Oue, M.; Kollias, P.; Matrosov, S.Y.; Battaglia, A.; Ryzhkov, A.V. Analysis of the microphysical properties of snowfall using scanning polarimetric and vertically pointing multi-frequency Doppler radars. *Atmos. Meas. Tech.* **2021**, *14*, 4893–4913. [CrossRef]
24. Doviak, R.J.; Zrnić, D.S. *Doppler Radar and Weather Observations*; Academic Press: London, UK, 1984.
25. Cao, Q.; Hong, Y.; Qi, Y.; Wen, Y.; Zhang, J.; Gourley, J.J.; Liao, L. Empirical conversion of the vertical profile of reflectivity from Ku-band to S-band frequency. *J. Geophys. Res. Atmos.* **2013**, *118*, 1814–1825. [CrossRef]
26. Japan Meteorological Agency Home Page. What is Graupel? About Rainfall and Snowfall, Questions and Answers. Available online: https://www.jma.go.jp/jma/kishou/know/faq/faq1.html (accessed on 6 November 2023). (In Japanese)
27. Kajikawa, M. Observation of density of graupel particles. *Tenki* **1976**, *23*, 685–695. (In Japanese)
28. Maruyama, H. On Conical Graupel and its Density. *Pap. Meteorol. Geophys.* **1968**, *19*, 101–108. [CrossRef] [PubMed]
29. Ray, P.S. Broadband Complex Refractive Indices of Ice and Water. *Appl. Opt.* **1972**, *11*, 1836–1844. [CrossRef] [PubMed]
30. Zhang, G. *Weather Radar Polarimetry*, 1st ed.; CRC Press, Inc.: Boca Raton, FL, USA, 2016.
31. Japan Meteorological Agency Home Page. Historical Weather Data Search. Available online: https://www.data.jma.go.jp/stats/etrn/upper/index.php (accessed on 6 November 2023). (In Japanese)
32. Hong, S.; Lim, J.O.J. The WRF Single-Moment 6-Class Microphysics Scheme (WSM6). *Asia-Pac. J. Atmos. Sci.* **2006**, *42*, 129–151.

Disclaimer/Publisher's Note: The statements, opinions and data contained in all publications are solely those of the individual author(s) and contributor(s) and not of MDPI and/or the editor(s). MDPI and/or the editor(s) disclaim responsibility for any injury to people or property resulting from any ideas, methods, instructions or products referred to in the content.